Evaluation of Factors Affecting the Performance of Fiber-Reinforced Subgrade Soil Characteristics Under Cyclic Loading

Frank I. Aneke [1]*, Shadi Hanandeh [2], Denis Kalumba [3]

[1] *Geotechnics and Materials Development Research Group (GMDRg) Civil Engineering, University of KwaZulu-Natal, Durban 4004, South Africa.*

[2] *Associate Professor, Department of Civil Engineering, Al-Balqa Applied University, Salt, 19117 Jordan.*

[3] *Department of Civil Engineering, University of Cape Town, Cape Town, South Africa.*

Abstract

This study is focused on evaluating the factors affecting the performance of fiber-reinforced subgrade under cyclic loading. To achieve the objectives of this study, a series of dynamic triaxial (DT) tests was performed, and the following parameters, such as resilient modulus (M_R), number of loading cycles (N), cyclic stress (CS), resilient strain (RS), and stress-strain hysteresis response of both the reinforced and unreinforced subgrades were evaluated. Subsequently, a series of scanning electron microscope (SEM) tests was conducted to track the fiber-soil interfacial bonding after the completion of DT test. The results indicated that N and CS triggered an appreciable decrease in M_R with significantly high RS deformation for the unreinforced subgrade. However, reversed responses were noted upon the inclusion of sisal fiber due to fiber-soil adhesion and a high ductility response was portrayed by the reinforced subgrades. A reversed response was significant upon 0.25% and 0.5% fiber inclusion, beyond which the CS resistance slightly decreased. The stress-strain hysteresis loop was observed to increase as the axial strain increased proportionally with an increase in fiber contents, thus causing a significant increase in energy absorption in specimens. The SEM micrograph showed tightly knitted fiber-soil adhesion after the DT test. This study indicated that the reinforced subgrade sustained the CS, N, and improved energy absorption capacity, and M_R upon fiber inclusion.

Keywords: Resilient Modulus; Hysteresis Loop; Sisal Fibre; Cyclic Stress; Subgrade.

1. Introduction

The subgrade soils experience traffic-induced stress throughout their service life and most times fail to sustain this stress due to their particulate nature. Most times pavements deteriorate occur as a result of the subgrade to sustain cyclic-induced stress from the traffic loading. Though, subgrades are known to accumulate cyclic stress at the initial stage of cyclic loading. Hence, the subgrade becomes elastic and gradually loses its recoverable strain capacity as the number of stress cycles increases, leading to crack formations and eventually deterioration of the pavement structure [1, 2]. Also, a few studies have supported the idea that cyclic stress is an externally generated force with great impact that negatively affects the internal structure of the subgrade particle [3–5]. Overall, the deformation resistance of fiber-reinforced subgrade soil is an important input parameter required to analyze the performance of pavement structure against dynamic, impulsive, and cyclic stress from traffic loads [6, 7]. Therefore, resisting the subgrade resilient deformation by sustaining cyclic stress to confine cracks and distress of the entire pavement structure is one such gap this study intends to bridge using the concept of interfacial friction and adhesion, which directly affect the contact area of soil/fiber matrix.

The deformation of subgrade soil under cyclic loading is important to analyze using the concept of soil dynamic behavior. The cyclic stress contributes to the deformation of subgrade soil, which eventually causes the complete collapse of the pavement structure before the end of its service, as indicated by [8–13]. It is also a fact that cyclic stress is one of the major factors that affect the performance of pavement structures, and its deformation is very important to understand. Guo et al. [14] indicated in their study that the deformation response of subgrade soil under cyclic loading is quite different compared to that of static loading. Cai et al. [15] suggested that the challenges of subgrade behavior under cyclic loading have become more serious due to the dynamics of cyclic stress on the subgrade. Hence, analyzing a pavement structure using the concept of static loading would result in great design errors. Because the long-term accumulation of lower-strain energy in the subgrade could trigger complete pavement failure [16]. Therefore, the long-term accumulation of lower-strain energy by the subgrade must be considered a serious threat. Qiu et al.'s [17] research on the performance of reinforced subgrade subjected to cyclic loading to resist cracking is gaining widespread attention. The soil reinforcement technique with randomly distributed fibers has been extensively reported in the literature [18–20]. Utilizing randomly distributed elements such as natural fibers, discontinuous multi-oriented polypropylene elements, metallic fibers, synthetic fibers, and polymeric mesh elements. The fiber reinforcing technique has proven to be effective in different geotechnical projects such as subgrade, retaining structures, slope embankments, and earth dams, resisting tension and cyclic stress that are capable of inducing soil failure.

Seed & Idriss [21] investigated the deformation response of a few cohesive soils under cyclic loading and developed a model relationship between cyclic loading and deformation. They concluded that the influence of repeated stress depends on the degree of compaction and the age of the subgrades at which the testing was conducted. AASHTO [22], the American Association of State Highway and Transportation Officials, indicated in their report that flexible pavements experience frequent cyclic stress phenomena under the action of traffic loads. They further concluded in their data analysis that the plastic deformation of the subgrade was the major cause of pavement deflection due to the irrecoverable strain pattern of the subgrade. Brown & Hyde [23] supported the idea that the accumulated plastic strain rate of the subgrade was significantly affected by the ratio of dynamic stress to that of confining pressure. Ling et al. [24] reported on the correlation between residual strain and pore pressure of subgrade soil under traffic loading in an indoor dynamic triaxial test. Their study also estimated the pattern of residual deformation for soft subgrades subjected to traffic loading. Their study suggested that the intensity of traffic loading has a significant influence on the strain and pore pressure of subgrade soil, particularly for subgrade with shallow depth. Mazari et al. [25] demonstrated that subgrade specimens fabricated using the same compaction energy exhibited the same deformation response; for instance, the deformation rate of the subgrade increased with a given increase in moisture content. They concluded that after cyclic loading, the deformation modulus and stiffness of the subgrade decreased with an increase in permanent deformation.

Though some progress had been made in the dynamic stress accumulation of subgrade soil under cyclic loading, Yang et al. [26] conducted a field test and numerical simulation for the spatial distribution and accumulative effect of dynamic stress. The field monitoring tests and model simulation recorded the relationship between dynamic stress accumulation in subgrade soil and the number of loading cycles. Both the model and field test results pointed out that subgrade permanent deformation occurred at high cyclic stress due to accumulated strain, irrespective of the subgrade thickness. In addition, Tevakumar et al. [27] examined the relative influence of cyclic stress ratio (CSR) and frequency on the response of soft subgrade subjected to high cyclic stress to simulate repeated train loading. To achieve the objective stated in their study, they combined the traditional cyclic triaxial test results with those obtained from the dynamic hollow cylinder apparatus. A series of cyclic undrained laboratory tests were performed on reconstituted sandy clay specimens at varying frequencies (f = 0.1–1 Hz) and cyclic stress ratios (CSR = 0.2–0.3). It was concluded that the hollow cylinder test results showed that higher CSR values and lower frequencies triggered higher permanent deformations and excess pore water pressures at a given number of load cycles. Available works of literature have suggested that subgrades have a certain level of threshold stress, beyond which cyclic stress induces permanent irrecoverable shear deformation on the subgrade even at high compaction energy.

However, not much has been reported on the resilient modulus (cyclic stress, number of load cycles, and stress-strain hysteresis response of reinforced subgrade soil). It is therefore imperative to fill this knowledge gap so that informed decisions and technical insight can be established on the applicability of sisal fibers in pavement construction for cyclic stress distribution within the subgrade. In this study, a sisal fiber of 30 mm in length and respective percentages of 0.25%, 0.5%, and 1.0% were used to reinforce reconstituted subgrade soil. The cyclic behavior of the fabricated subgrade soil was measured by performing a series of dynamic triaxial (*DT*) tests, followed by a series of SEM tests to analyze fiber-soil adhesion after the *DT* test. The effects of random inclusion of fiber were evaluated against some factors such as resilient modulus (M_R), number of loading cycles (*N*), cyclic stress (*CS*), resilient strain (*RS*), and stress-strain hysteresis response. The obtained results showed that fiber-reinforced specimens accumulated and sustained several loading cycles, thereby providing significant resistance against deformation and resilient strain up to a limiting fiber content of 0.5%, beyond which the resistance decreased with microcrack formation.

2. Materials and Experimental Program

2.1. Soil

The bulk sample of the subgrade soil was obtained from the Pietermaritzburg area of Kwazulu Natal in South Africa. A trial pit of approximate size 1.6 m by 1.3 m was manually dug, and natural subgrade soil was sampled at 1.2 m collected. The collected soil sample was oven-dried for 24 hours following particle size batching to avoid particle size discrepancies that could affect test results. The particle size distribution analysis was performed following the ASTM D1140 [28] protocol, and the grading curve of the soils is shown in Figure 1. The soils that passed through the 0.075mm sieve size were further subjected to a hydrometer test to measure the percentages of silt and clay for the representative subgrade soils.
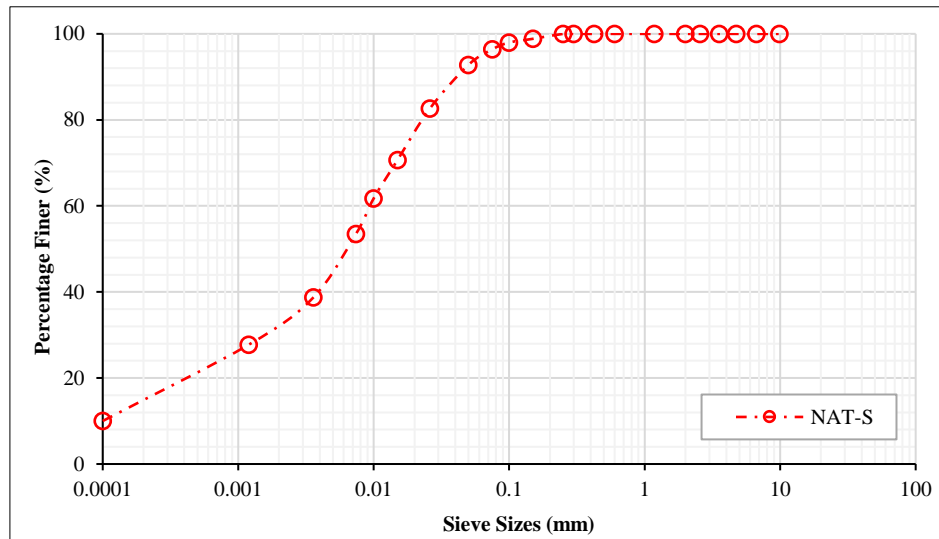

Figure 1. Soil gradation curve

The collected subgrade materials have cumulative percentages of soil particles passing through the ASTM sieve size of 200 varying between 75% and 100%. Also, consistency limit tests were performed following the ASTM D4318-17e1 [29] testing procedure. The test results revealed that the soil had a liquid limit of 48% and a corresponding plasticity of 31%. Based on the obtained test results, the collected subgrade material is identified as clay with low plasticity (CL) soils according to the Unified Soil Classification System (USCS). It is found that the subgrade soil has oxides (alumina, silica, and iron oxides) as the dominant oxides, contributing to 89.71 percent of the chemical composition. Thus, a detailed summary of the subgrade material index and chemical composition is presented in Table 1.

Table 1. Summary of soil properties used for the study

Soil properties	Values
Specific gravity	2.71
Shearing resistance angle (CU test)*	36^0
Consistency limits tests	
Liquid limit (%)	48
Plastic limit (%)	17
Plasticity Index	31
Linear shrinkage (%)	5.2
USCS	CL
Proctor test	
Maximum dry unit weight (kN/m^3)	20.21
Optimum moisture content (%)	16.24
Mineral composition (%)	
Al_2O_3	14.37
CaO	2.25
SiO_2	54.10
Fe_2O_3	17.34
MgO	0.42
K_2O	3.75
pH	7.51

* CU: Consolidated Undrained

2.2. Natural Fiber

The fiber used herein was supplied by Uni-Cord SA as a rope. The fiber ropes were oven-dried at 38°C for 9 hours. The fibers were notched to the desired length of 30 mm using a sharp knife. A steel ruler was used to measure the fiber length during the cutting exercise to minimize length disparities that might affect the accuracy of the results. Subsequently, an average of three fiber tensile tests were conducted following ASTM D3822 [30] protocols to measure the mechanical properties. Sisal fiber reduced strain-to-failure by 5.2 percent to 2.6 percent as gage lengths increased from 10 mm to 40 mm. The mean values of the tests were recorded as the final test results, and the detailed results for the sisal fiber are presented in Table 2.

Table 2. Properties of the sisal fiber used for the study

Fibre property	Value
Aspect ratio	100
Average diameter(mm)	0.3
Elongation at break (%)	2.3
Elasticity Modulus (GPa)	24
Breaking tensile strength (GPa)	0.56

3. Sample Preparation

The maximum dry density and the corresponding optimum moisture contents of the soil-fiber composite were measured according to ASTM D-698 [31] testing procedures. The expression in Equation 1 was applied to evaluate the percentage of sisal fiber in the specimens.

$$\rho = \frac{\theta_f}{\theta_s} \tag{1}$$

where, θ_f is the total fiber mass and represents the soil mass. Fibre contents of 0.25%, 0.5%, 0.75%, and 1.0% were used in this study. The preparation of the specimen followed a sequential procedure. Firstly, a known quantity of the subgrade material was weighed out, and calculated fiber contents of 0.25%, 0.5%, and 1.0% were also obtained and kept in various dry containers. Each content was thoroughly mixed with the corresponding quantities of subgrade materials for 5 minutes under dry conditions. After dry mixing, quantities of water corresponding to the optimum moisture content (OMC) of 16.24% were added to the mixture until a consistent composite homogeneity was attained. The soil composite was allowed to mellow for 2 hours in an airtight plastic bag before specimen fabrication, as further mixing continued for 15 minutes to prevent clumping of the soil composite during wet mixing. The marginal loss of moisture during specimen preparation was compensated by adding 1% (OMC) moisture content to the mellowed composite.

Immediately after mixing, the composite was placed into molds with a diameter of 150 mm and a height of 300 mm, followed by dynamic compaction. The soil composite was compacted into the molds using five layers with 16 blows, making a total of 80 blows for each specimen preparation, hence achieving a compaction energy of 1544 kN m³/m³. The method of compaction was selected due to the height of the mold as well as to achieve a highly compacted composite suitable for dynamic triaxial testing. The compaction energy was calculated using the mathematical expression in Equation 2.

$$E_c = \frac{WN_BN_LH_D}{V} \tag{2}$$

Hence, the fabricated specimens were certified suitable for testing when the dry density of the specimens was at least 98% close to the control dry density. The fabricated specimens were eventually placed in the curing chamber and allowed to cure at a temperature of 38°C for 14 days. This curing condition was selected due to the sensitive temperature changes of the lignocellulosic polymer content of sisal fibers [32]. Though the mechanical properties of sisal fibers degrade, they are certified to deteriorate at temperatures around 200°C. since the curing temperature of 38°C was sufficiently below the glass transition temperature of the lignocellulosic polymers for sisal fiber. It was ascertained that the sisal fiber was not subjected to any morphological changes throughout the curing period.

4. Experimental Procedure

The experimental procedure of this study is demonstrated using the flowchart diagram shown in Figure 2. The flowchart diagram illustrates the methodological process followed to achieve the objective of this study. According to the flowchart diagram, the subgrade soil was mixed with sisal fiber under the conditions before the calculated quantity of water was added, and the blend was mixed for 15 minutes until a homogeneous mix was achieved. Subsequently, the geo-composite was fabricated into various sizes and shapes using a compaction test, after which the dynamic triaxial and SEM tests were conducted following the ASTM standard protocols. The data for each was collected, and the results were interpreted.
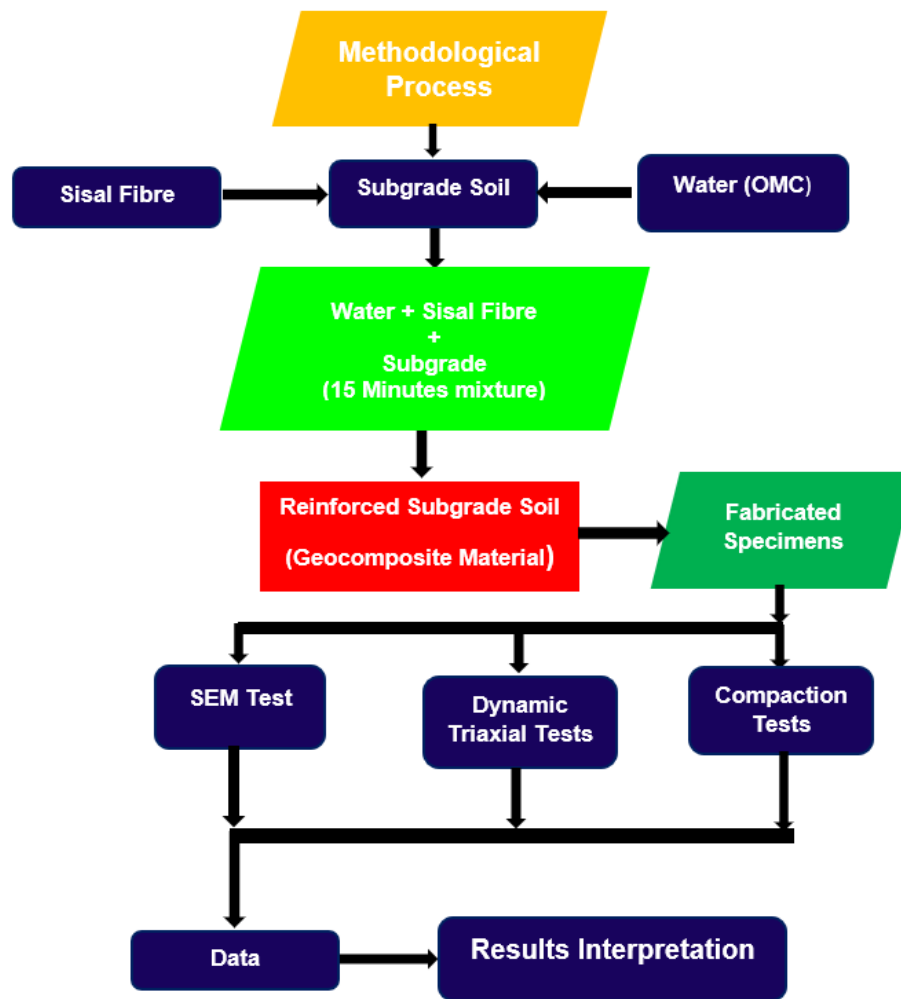
Figure 2. Flowchart for the methodological process followed

The dynamic compaction test was achieved following the ASTM D698 [31] standard protocols. The specimens were fabricated using a compaction energy of 1544 kN-m/m^3. An automated compaction machine was used in this study to maintain uniformity in shape, size, and compaction energies throughout the specimen fabrication. Dynamic Triaxial testing was performed to evaluate strength and deformation properties under cyclic loading conditions on the fabricated composites. There are many variations of DTT; however, the traffic loads on highway subgrade are characterized by low amplitude and high cyclic stress. The tests were performed using the Dynatrax cyclic triaxial test device, and the fabricated specimens are shown in Figure 3. Therefore, the loading sequence of AASHTO T307-99 [33] was followed, considering the actual field cyclic stress on the subgrade. First, the specimens were preconditioned by applying 1000 cycles, followed by 100 cycles for every sequence. The cyclic loading at the constant strain of 0.1 and frequency of 10 Hz was applied coupled with confining pressures of 20, 50, and 100 kPa, and the test data (resilient modulus, cyclic stress, and stress-strain hysteresis loops) were processed through data acquisition software that runs on a personal computer with a Windows operating system. The average permanent strain was determined as the average strain of the first cycle according to recommendations by Vucetic & Mortezaie [34].
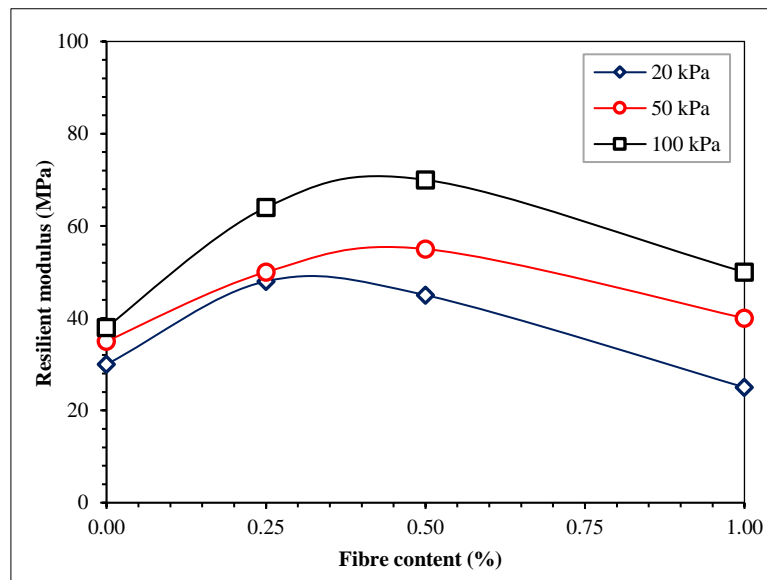

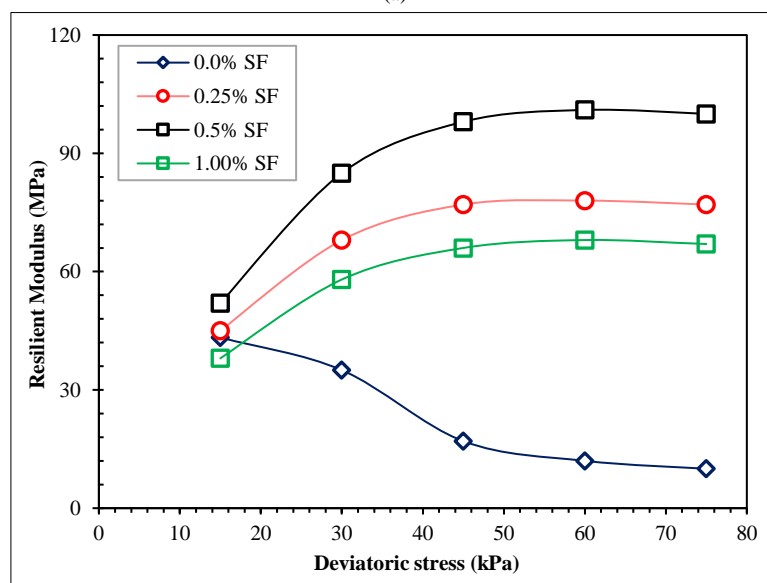**Figure 3. Dynamic triaxial test device and fabricated subgrade soil**

5. Results and Discussions

5.1. Effects of Fiber Inclusion on Resilient Modulus

The effects of fiber contents on the resilient modulus of the reinforced subgrade at various confining pressures are shown in Figure 4-a. The test result confirmed that increasing the fiber content caused an appreciable increase in resilient modulus values to a limiting fiber content of 0.5%, beyond which the resilient modulus slightly decreased. Also, it was noted that the increase in confining pressure mobilized increased the resilient modulus value of the reinforced subgrade. The unreinforced specimens recorded resilient modulus values of 30 MPa, 35 MPa, and 38 MPa at confining pressures of 20 kPa, 50 kPa, and 100 kPa, respectively. The resilient modulus of the unreinforced specimens at a confining pressure of 100 kPa increased from 38 MPa to 0 MPa upon the addition of 0.50% fiber content. Whereas, with the same fiber content of 0.50%, at confining pressures of 20 kPa and 50 kPa, respectively. The resilient modulus increased from 30 MPa to 45 MPa and from 35 MPa to 55 MPa, thereby causing a 50% and 57% increase in the resilient modulus, respectively. An increase in confining pressure mobilized the adhesion of the soil-fiber interface and improved the cyclic stress resistance of the reinforced subgrade. The results inferred that both the fibers and confining pressure augment the stiffness of the subgrade soil. The resilient modulus of the reinforced subgrade gradually improved as fiber contents increased sequentially from 0.25% to 0.5%, beyond which the resilient modulus values decreased. The decrease in resilient modulus value is caused by the increase in the volume of fibers, which in turn triggers changes in the volume of soil and void within the composite. This phenomenon is common because sisal fibers possess a low unit weight of 1.5 g/cm^3 [35].
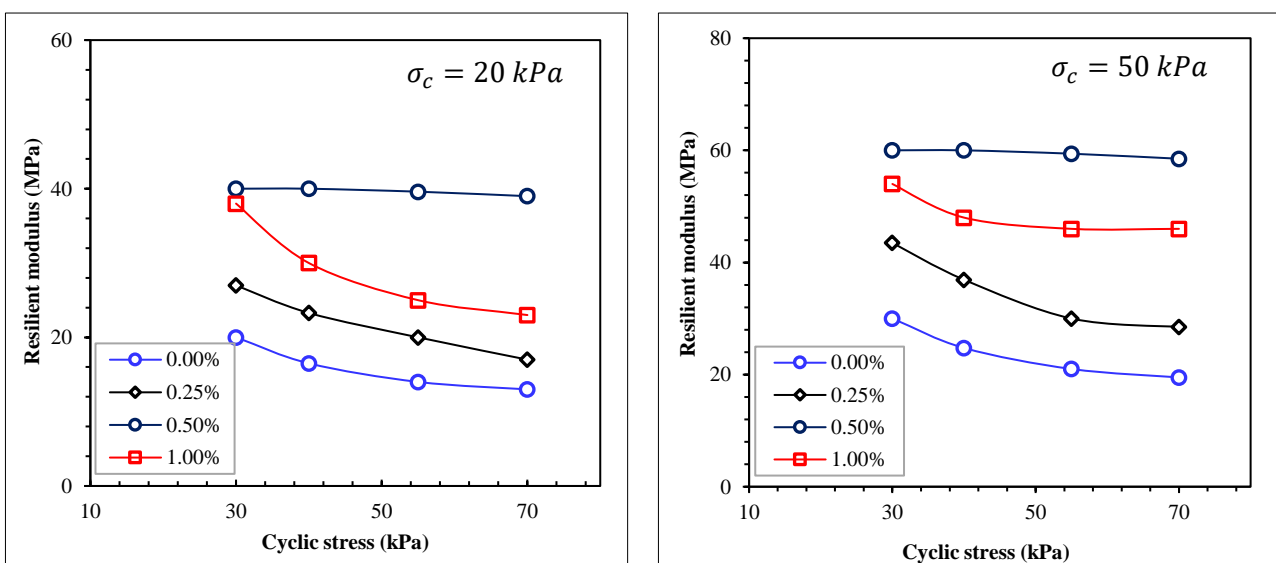

(a)

(b)

Figure 4. a) Variation of resilient modulus with fiber content, b) Effects of sisal fibre on the Variation of M_R with deviatoric stress at 100 kPa of confining pressure

Similarly, Figure 4-b demonstrates the impact of sisal fiber on the variation of resilient modulus with cyclic deviatoric stress. Though the variations between the resilient modulus and the deviator loads indicate that the unreinforced subgrade failed to resist the increase in deviator stress, which is considered to occur due to the strain softening as supported by Mazari et al. [25]. The result indicated that the main effects of deviatoric stress are significant on unreinforced subgrade soil. Also, the result proves that confining stresses have more positive influences on resilient modulus compared to deviator stresses. It was also noted that at low levels of cyclic deviatoric stress, the resilient modulus increased slightly but stabilized without any further decrease in resilient modulus even as the deviatoric stress increased [36–39]. This is attributed to the strain hardening of the specimen mobilized by the confining pressures and sisal fiber. The results obtained in this section imply that the optimum content of sisal fiber is required to reinforce the weak subgrade investigated in this study. Also, the fiber-reinforced subgrade sustained the cyclic stress intensity, and it eventually resisted cracking.

5.2. Effects of Cyclic Stress on Resilient Modulus

The variation of resilient modulus at different cyclic stresses of 30 kPa, 40 kPa, 55 kPa, and 70 kPa on reinforced and unreinforced subgrade soils is shown in Figures 5. It is indicated that increasing cyclic stress significantly affected resilient modulus values for unreinforced subgrade soils. Thus, at 30 kPa of cyclic stress level, the unreinforced subgrade sustained the stress, though it was observed that the resilient modulus decreased swiftly without any resistance as the cyclic stress moved from 40 kPa to 70 kPa. On the other hand, the resilient modulus of the 0.25% reinforced subgrade was recorded to slightly decrease by 12% as the cyclic stress increased from 55 kPa to 70 kPa. The observed decrease in resilient modulus with cyclic stress is due to the nonlinearity of the soil stress-strain correlation. Furthermore, the 0.5% fiber-reinforced subgrade soils demonstrated strong resistance against cyclic stress, as no decrease in resilient modulus was recorded from low to high cyclic stress levels. An appreciable decrease in resilient modulus was noted for the 1.0% fiber-reinforced subgrade, and an average decrease of 55.2% in resilient modulus was obtained compared to the 0.5% fiber-reinforced subgrade. The decrease in resilient modulus for 1.0% reinforced subgrade was possible due to the fiber-fiber interface within the soil matrix, as weak bonding between the soil matrix and fiber was developed.

Previous studies by Głuchowski & Sas [40] and An et al. [41] have suggested that soil stiffness is high at low cyclic stress levels but decays with an increase in high cyclic stress levels. In addition, their studies supported the fact that strain level increases with cyclic stress, hence resilient modulus decreases with an increase in cyclic stress. Furthermore, most published studies have shown that resilient modulus decreases with cyclic stress increase [42]. On the contrary, the results obtained in this study revealed that the resilient modulus remains at equilibrium as the cyclic stress increases for the reinforced soils. Whereas a significant decrease in resilient modulus was noted as the cyclic stress increased for the unreinforced subgrade soil. The test results obtained in this investigation are in line with a study published by Xie et al. [43]. The fiber inclusion improved the resilient modulus of the reinforced subgrade and sustained cyclic stress even at the high-stress level. Hence, this is attributed to the interweaving of the fiber, which in turn restrained the soil matrix from undergoing significant deformation at high cyclic stress.
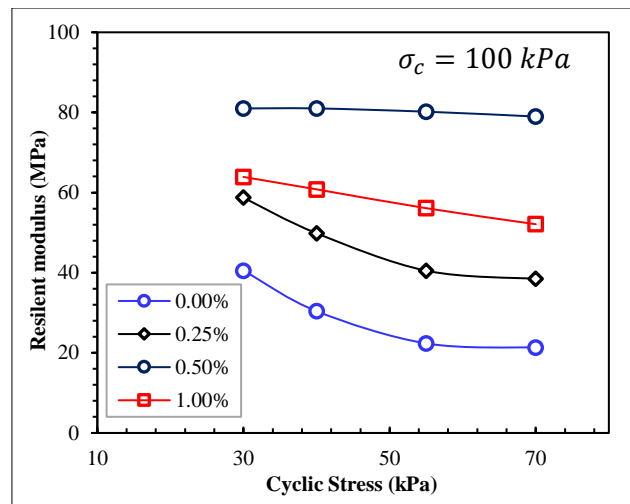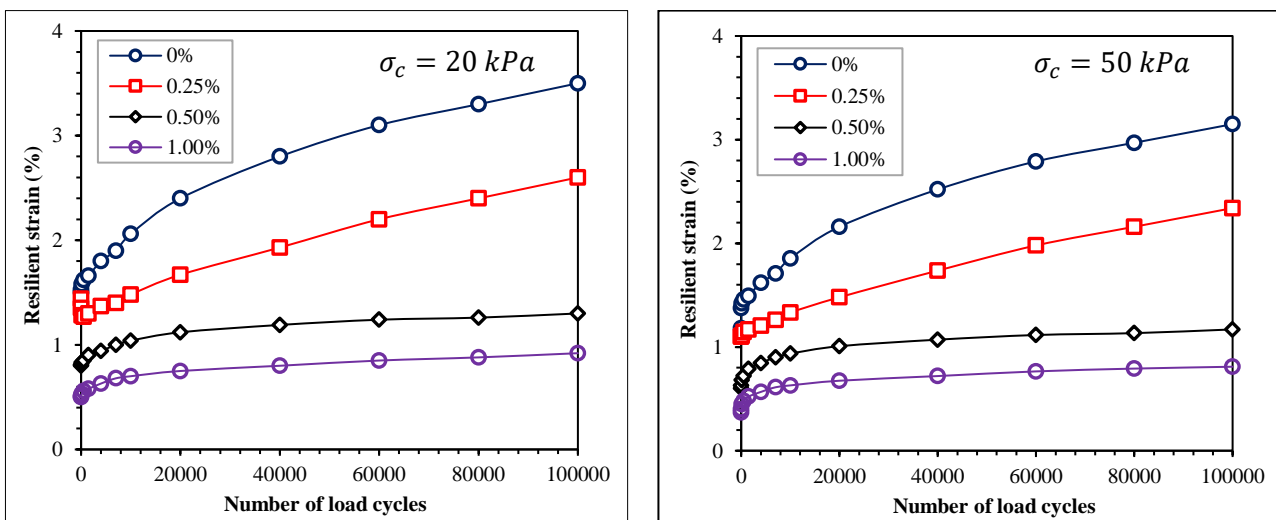
Figure 5. Variation of cyclic stress with resilient modulus for reinforced and unreinforced subgrade soil

5.3. Effects of Loading Cycles on Resilient Strain

The variation of resilient strain under a repeated cycle number of 100,000 for reinforced and unreinforced subgrades at various confining pressures is shown in Figure 6. The test results revealed that the resilient strain increased as the number of loading cycles increased for unreinforced subgrade soils. The unreinforced subgrade soil recorded an average resilient strain of 0.3%, whereas the reinforced subgrade soil recorded a resilient strain of 0.05%. The test results implied that unreinforced subgrade soils exhibited a high rate of strain deformation compared to the reinforced specimens. At the initial stage of the loading cycles between 0 and 1,000 cycles, the unreinforced specimens marginally sustained the loading intensity as the resilient strains remained unchanged. The unreinforced subgrade soil ceased to sustain the intensity of the loading cycles between 2,000 and 100,00, hence causing an exponential increase in resilient strain from 1.8% to 4%. For the reinforced subgrade soils, the resistance of resilient strain is more consistent, such that a slight difference was observed between the start and the end of the loading cycles. This implies that the reinforced subgrade soil sustained a greater number of load cycles with a slight increase in resilient strain. It was noted that the resilient strain impact was noted on the specimens reinforced with 0.25% sisal fiber compared to the subgrades reinforced with 0.5%. Upon the inclusion of 1.0% sisal fiber, resilient strain accumulation was noted from the initial stage until the end of the loading cycles. However, the strain accumulation was mobilized due to the effect of sisal fiber stiffness within the soil matrix.

The indicated behavior of the fiber-reinforced subgrade soil agrees with the results reported elsewhere by Sandjak & Tiliouine [44] and Tang et al. [45]. This behavior was also reported by Bian et al. [46]. The confining pressure slightly increased the stiffness of the unreinforced subgrade soil. This mobilized a minor improvement in the resilient strain resistance properties. In addition, confining pressures significantly enhanced the adhesion of the soil-fiber interface and improved the resilient strain resistance of the reinforced subgrade soil due to the mechanical interlock of the fibers and soil particles. Generally, fiber inclusion enhanced the resilient strain resistance of the subgrade and improved the energy-absorbing properties of the composite, which prevented it from de forming. The resistance to cyclic deformation was enhanced by a gradual increase in fiber content; thus, this ultimately led to the accumulation and sustenance of loading cycles, hence causing the resistance to the deformability of resilient strain.
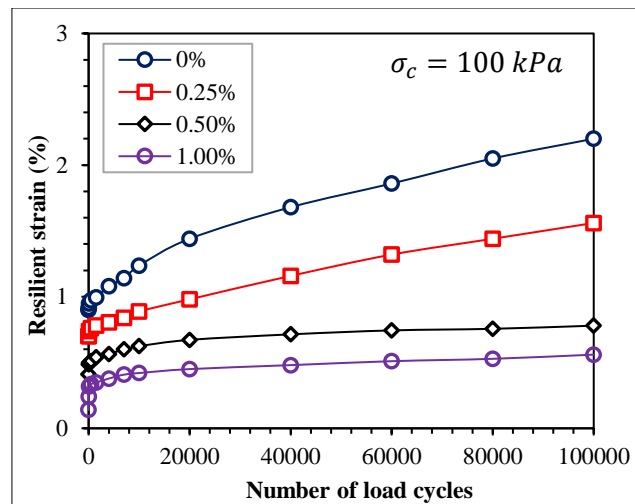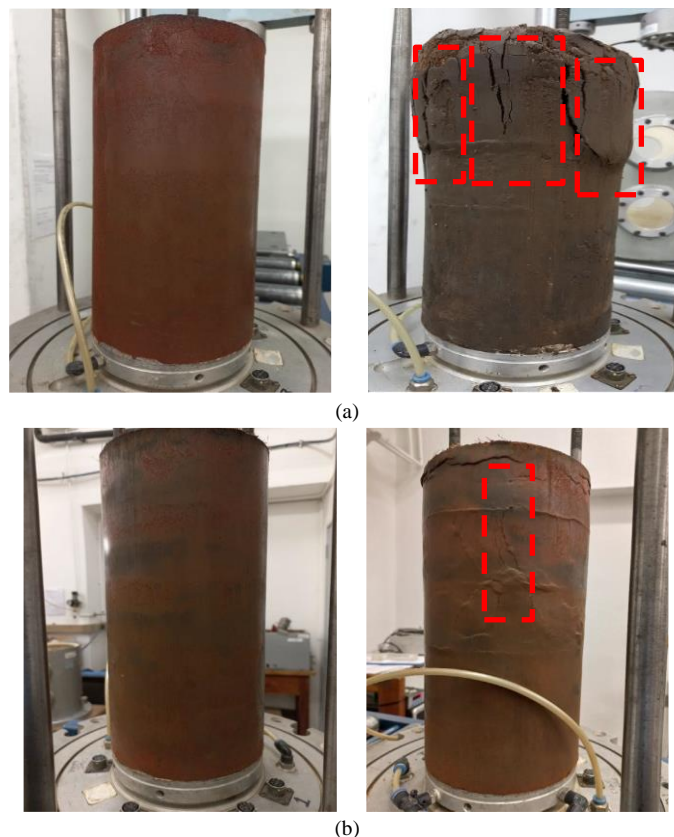
Figure 6. Variation of resilient strain with the number of loading cycles for reinforced and unreinforced subgrade

Furthermore, the number of load cycles shown in Figure 7-a depicts that the unreinforced subgrade soil recorded a complete collapse at 2,000 loading intensities. However, there is some resistance recorded by the unreinforced subgrade at the initial stage of the loading cycle. Hence, the unreinforced specimens failed to sustain the loading intensity as the number of load cycles increased, causing large resilient strain and eventually significant deformation. Meanwhile, the 0.25% fiber-reinforced specimens sustained the intensity of the loading cycles starting from 0 to 100,000 cycles with little manifestation of microcracks on the specimen upon test completion, as shown in Figure 7-b. This indicated a 65% crack reduction was achieved upon 0.25% inclusion of sisal fiber compared to the unreinforced specimens on average. Furthermore, no form of crack was found on the specimens reinforced with 0.5% sisal fiber, as demonstrated in Figure 7-c. This simply implies that 0.5% of sisal fiber is the optimum percentage required to resist a crack at high train energy with little resilient strain energy of less than 0.05%. In addition, Figure 7-d depicts the condition of the tested subgrade specimens before and after the dynamic triaxial test for a 1.0% sisal fiber-reinforced subgrade. It can be shown that the specimens revealed a minimum level of cracks that was less than 8% compared to the unreinforced specimens. Generally, the level of crack revealed is directly proportional to the percentage of sisal fiber the specimens contained. Judging from the 1.0% inclusion of sisal fiber, the specimen experienced what is known as a fiber cluster within the matrix of the specimen. Hence, not allowing sufficient space for soil-fiber interaction but rather portraying fiber-fiber interfacial bonding. This conforms to studies by Han et al. [47] and Estabragh et al. [48], which stated the subgrade crack is mobilized by the shaped particle of the soil and compaction effort.
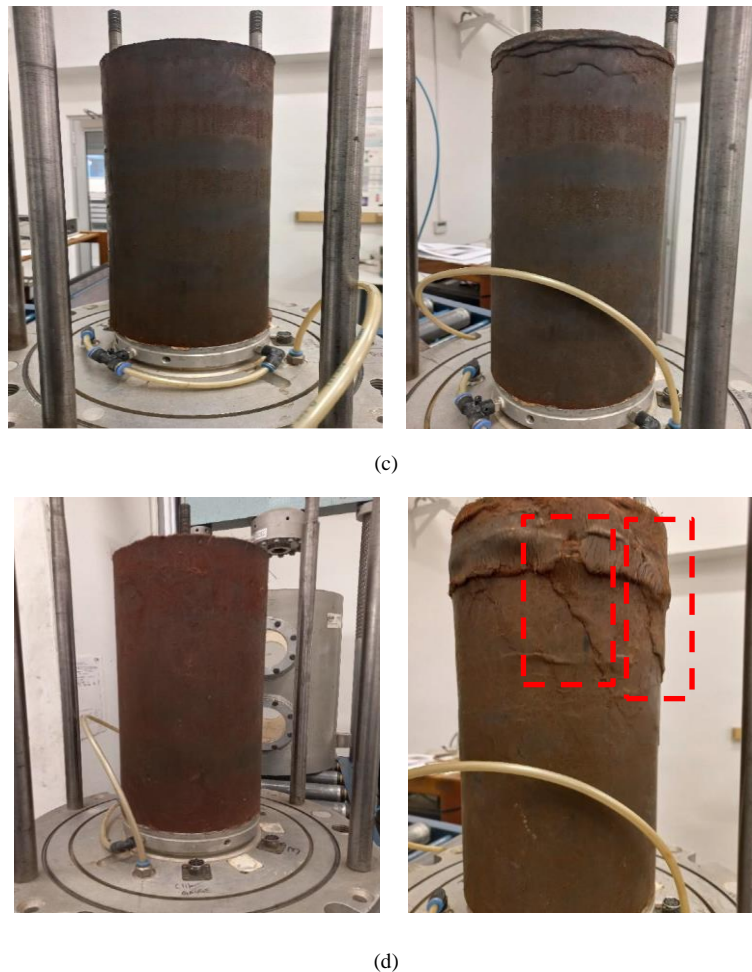

(a)

(b)

(c)

(d)

Figure 7. a) Before and after cyclic loading testing of the unreinforced specimens, b) Before and after cyclic loading testing of the 0.25% fibre-reinforced specimens, c) Before and after cyclic loading testing of the 0.5% fibre-reinforced specimens, d) Before and after cyclic loading testing of the 1.0% fibre-reinforced specimens.

5.4. Effects of Fiber Contents on the Stress-Strain Hysteresis Loop

The stress-strain hysteresis loops of reinforced and unreinforced subgrade soils for the final 5 cycles at various confining pressures are shown in Figure 8. It was noted that the shear stress increased significantly at the early stage of cycle number; however, this increment gradually became sustained at the 1000th cycle for the reinforced subgrade soil. It is evident from the curves that the loops are more asymmetrical on both the compression and tension sides of the loops. The loops were densified as the strain level increased with an increase in cycle numbers, indicating the improved stiffness of the specimens. Under high applied strain levels, hysteresis loops become more asymmetrical, as supported by Kumar et al. [49]. The asymmetrical shape of the loops in this study is associated with the high strain level during cyclic shearing. The peak stress is the maximum shear stress in each hysteresis loop; accordingly, the reinforced subgrade exhibited a shear hardening response due to soil-fiber interfacial bonding under constant and cyclic normal loading, contrary to the unreinforced soils. The stress-strain hysteresis loop indicated that an increase in cyclic loading resulted in stronger restraint against sliding, rolling, and rotation of particles, resulting in greater shear stress due to the interlocking adhesion of the soil particles and fiber. The result obtained in this study agrees with the report published by Soliman and Shalaby [50] and Madhavi Latha et al. [51]. The shear stress in shear paths for the unreinforced subgrade sustained axial strain between 0 and 0.0078, indicating a poor hysteresis loop, whereas the stress-strain of reinforced subgrades tends to move forward between axial strains of 0.002 and 0.003, due to gained stiffness. Therefore, this is defined as the shear stress in the forward direction [52].
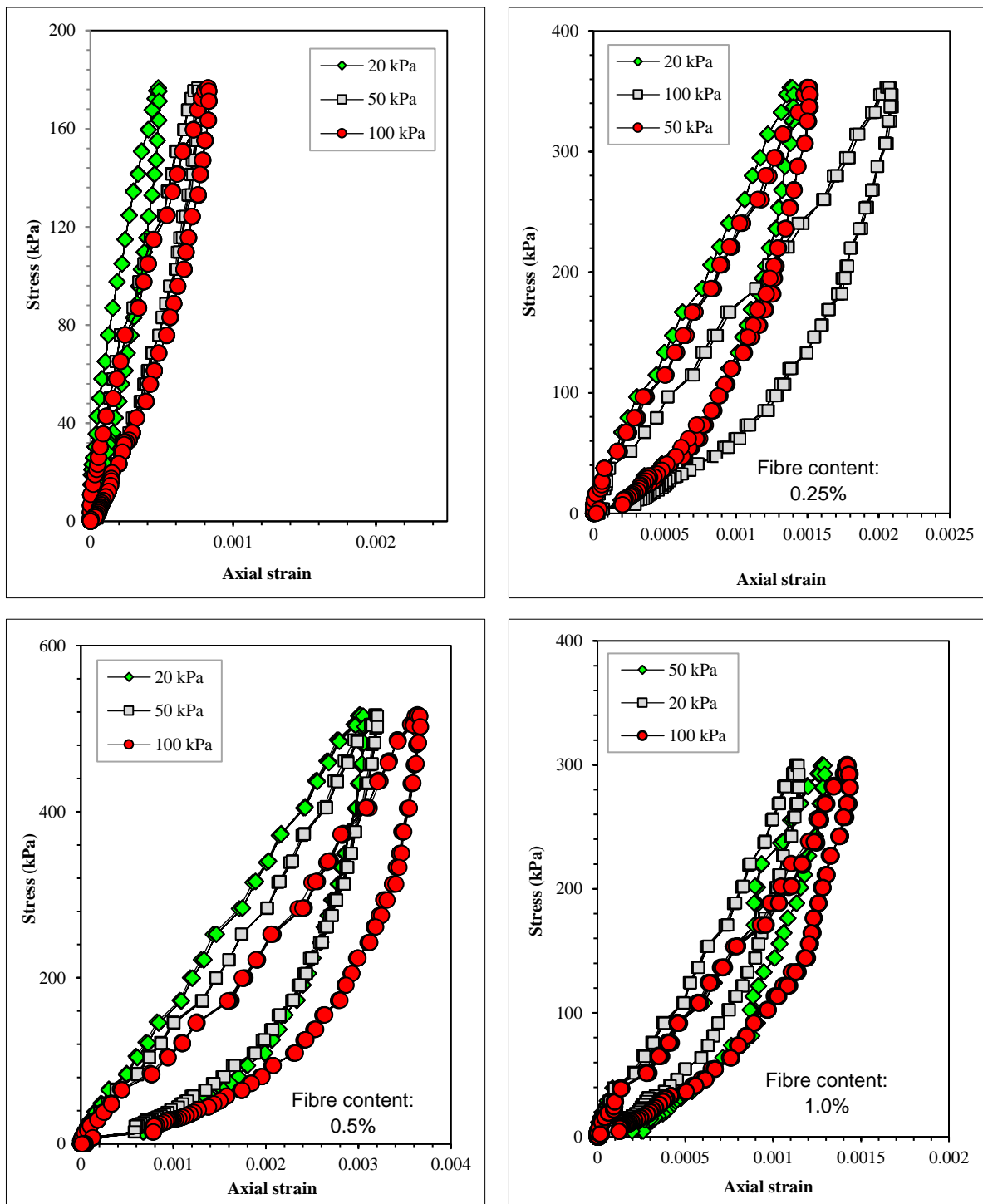
Figure 8. Hysteresis loop for unreinforced and reinforced subgrade soil at normal cyclic loadings

5.5. Morphological Analysis of Fiber-Soil Interface for Reinforced Subgrade Soils

The morphological analysis of the reinforced and unreinforced subgrades was performed using an SEM machine. The macroscale activities of the sisal fibers on the subgrade soil structure as well as the interfacial bonding were observed using SEM. The morphological micrograph of unreinforced and reinforced soil is presented in Figures 9-a to 9-d. The unreinforced subgrade soil (Figure 6) is primarily composed of a scattered pattern of particles. Also, void-like formations were identified within the matrix of unreinforced subgrade, justifying the rationale behind the degradation at high cyclic stress levels. The general random distribution of the fibers within the soil matrix (Figure 6). The micrograph portrayed demonstrates discrete fiber distributions within the matrix for 0.25%, 0.5%, and 1.0% of the fiber-reinforced soils. The micrograph indicated that the fiber acts like a three-dimensional network that interlocks with the soil particles. This forms an adhesive matrix, which restricts the resilient strain of cyclic stress. In furtherance, no deformation, debonding, or breakage of fibers was observed on the 0.25% and 0.5% fiber-reinforced specimens after the application of cyclic

stress. This behavior confirmed that the fibers within the soil matrix sustained damping and tension as well as overcame yielding while significantly resisting the deformation of the reinforced specimens. More so, this could be associated with the bond interfacial strength that is relative to mechanical interlocking friction along the fiber length. The friction between the fiber-soil interfaces was noted to be the dominant mechanism that controls the reinforcement micromechanical mechanism, as previously published by Olgun [53].
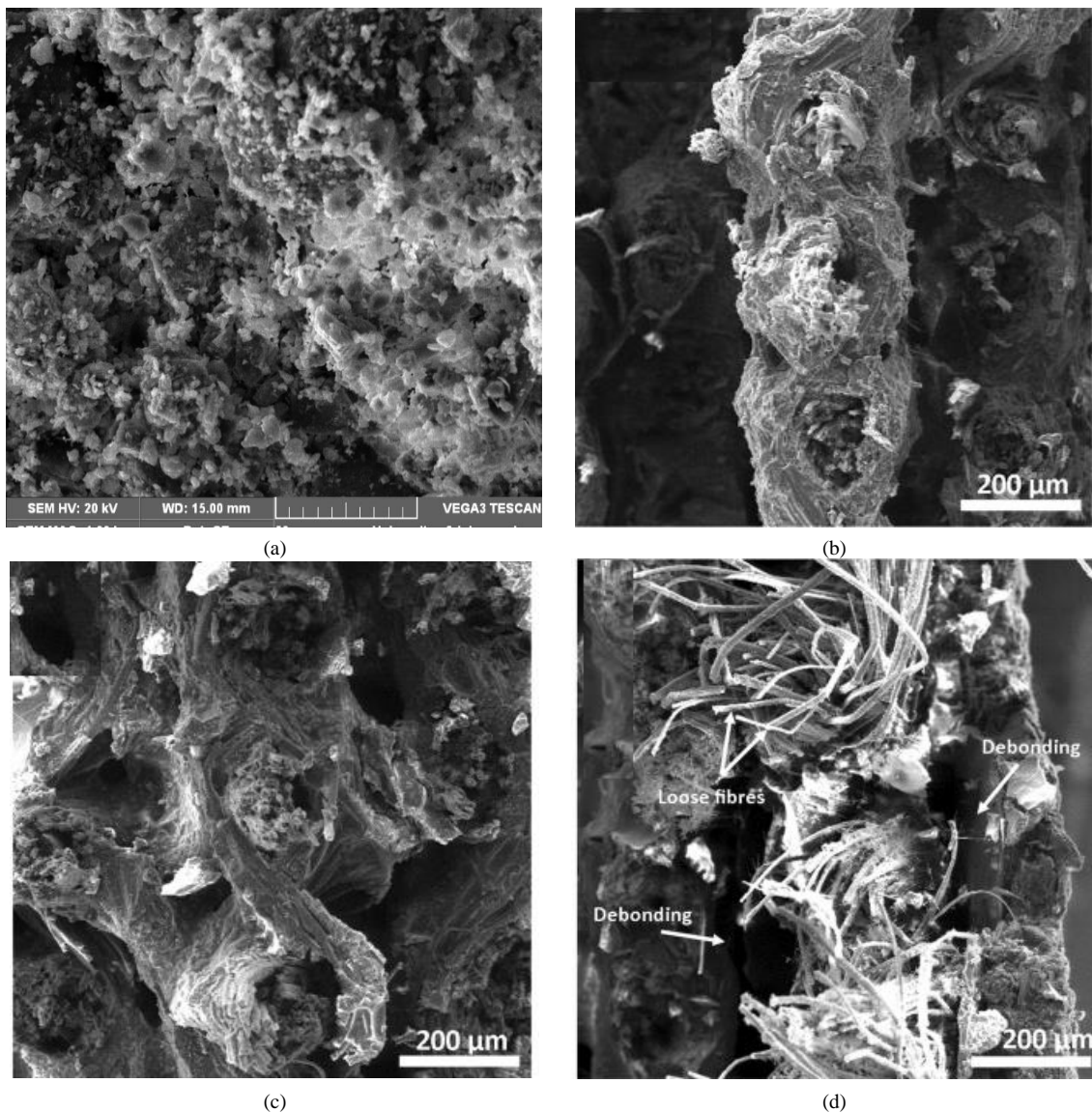

Figure 9. Micrograph of tested specimens (a) Unreinforced subgrade (b) 0.25% fiber-reinforced subgrade, Micrograph of test specimens (c) 0.50% fiber-reinforced subgrade (d) 1.0 % fiber-reinforced subgrade

However, debonding of fiber from the soil matrix was noted on the 1.0% reinforced specimens. The failure of the 1.0% fiber specimens is related to the magnitude content and the fiber-fiber interfacial forces. Due to the large content of fiber, the 1.0% fiber-reinforced soil embedding depth is small; hence, the effective contact area between the soil and fiber resulted in a larger interface action, causing ten failures. At the same time, this weakens soil stiffness and triggers the dispersion effect of fiber within the soil matrix, which has negative impacts on soil resistance against deformation. This result presented herein is similar to the results published by Gao et al. [54] and Tang et al. [55].

6. Conclusions

In this study, an assessment of the cyclic stress resistance of reinforced and unreinforced subgrade soils was investigated. Based on the obtained results, the following conclusion was drawn:

- The measured value of the subgrade soil increases with several load applications when the inclusion of 0.25% and 0.50% of sisal fiber is used to reinforce the subgrade; thus, the resilient modulus values significantly decrease in value as the discrete fiber content goes beyond 0.50% to 1.0% of fiber content. Furthermore, the deviatoric stress was noted to have no effects on the reinforced subgrade; on the other hand, the deviatoric stress induced

negative effects on the unreinforced subgrade and the 1.0% fiber-reinforced subgrade, indicating that the deviatoric stress is more pronounced in tension as the fiber content provided the required resistance against tension.

- Under cyclic loads, the resilient modulus of the unreinforced slab decreased as the number of load cycles increased. At the early stage of the loading cycles, the unreinforced subgrade increases exponentially as the number of loading cycles continues to increase. Unreinforced specimens failed to accumulate more loading cycles, therefore inducing higher resilient strain compared to reinforced subgrades that sustained the cycles of loading from low to higher stress levels.

- The resilient modulus of the unreinforced subgrades is found to be dependent on cyclic stress. Hence, it decreases with cyclic stress due to the nonlinearity of the subgrade soil stress-strain framework under cyclic stress. On the other hand, the resilient modulus values of the reinforced subgrade soils were sustained as the cyclic stress increased. The sustained resilient modulus values for the reinforced soil are noted as high-strain energy increases. This implied that the resilient modulus value of the reinforced subgrade was not. However, resistance against cyclic stress was visible at a confining pressure of 100 kPa because it induced additional fiber-soil interface adhesion as the interparticle forces between the soil and fiber increased, resulting in a stiffer composite.

- The fiber inclusions caused an increase in the shear stress hysteresis loop for specimens reinforced with 0.5% fiber content, beyond which the loop moved backward, causing poor resistance to the axial strain. The backward movement was attributed to the loss of stiffness of the reinforced soil due to the high percentage of voids created by the embedded depth of fiber, thereby causing a reduction in the effective contact area between the soil and fiber, which caused the tensile failure. This was identified by SEM micrograph as poor distribution fibers were indicated within the soil matrix, causing strength softening of the reinforced subgrade.

7. Declarations

7.1. Author Contributions

Conceptualization, F.I.A.; methodology, F.I.A.; software, F.I.A.; validation, S.H. and D.K.; formal analysis, F.I.A.; investigation, F.I.A.; resources, D.K.; data curation, S.H.; writing—original draft preparation, F.I.A.; writing—review and editing, S.H. and D.K.; visualization, D.K.; supervision, D.K.; project administration, F.I.A.; funding acquisition, F.I.A. All authors have read and agreed to the published version of the manuscript.

7.2. Data Availability Statement

The data presented in this study are available in the article.

7.3. Funding

7.4. Conflicts of Interest

The authors declare no conflict of interest.

8. References

[1] Ikechukwu, A. F., Hassan, M. M., & Moubarak, A. (2021). Resilient modulus and microstructure of unsaturated expansive subgrade stabilized with activated fly ash. International Journal of Geotechnical Engineering, 15(8), 915–938. doi:10.1080/19386362.2019.1656919.

[2] Ikechukwu, A. F., & Chibuzor, O. K. (2022). Improving resilient modulus and cyclic crack restriction of preloaded expansive subgrade treated with nano-geopolymer binder. Arabian Journal of Geosciences, 15(15), 1340. doi:10.1007/s12517-022-10629-x.

[3] Frank, A. I. (2015). Geotechnical properties of marginal highway backfill stabilized with activated fly ash. Master Thesis, University of Johannesburg, Johannesburg, South Africa.

[4] TANG, L. S., WU, Y. P., ZHAO, Z. L., ZHAO, L., & CHEN, H. K. (2019). Dynamic Stress Response Characteristics within Soil and Influence of pH under Cyclic Loading. Journal of Yangtze River Scientific Research Institute, 36(12), 78. doi:10.11988/ckyyb.20180622. (In Chinese).

[5] Ikechukwu, A. F., & Hassan, M. M. (2022). Assessing the Extent of Pavement Deterioration Caused by Subgrade Volumetric Movement Through Moisture Infiltration. International Journal of Pavement Research and Technology, 15(3), 676–692. doi:10.1007/s42947-021-00044-y.

[6] Aneke, F. I. (2018). Behaviour Of Unsaturated Soils for Road Pavement Structure Under Cyclic Loading. Ph.D. Thesis, Central University of Technology, Free State, Bloemfontein, South Africa.

[7] Ikechukwu, A. F., & Mostafa, M. M. H. (2020). Performance assessment of pavement structure using dynamics cone penetrometer (DCP). International Journal of Pavement Research and Technology, 13(5), 466–476. doi:10.1007/s42947-020-0249-z.

[8] Ikechukwu, A. F., & Mostafa, M. M. H. (2021). Assessing the coupling effects of nanosized fly ash and precompression stress towards mitigating subgrade cracks mobilised by traffic loading. Nanotechnology for Environmental Engineering, 6(3), 63. doi:10.1007/s41204-021-00157-6.

[9] Aneke, F. I., Mostafa, M. M. H., & El Kamash, W. (2021). Pre-compression and capillarity effect of treated expansive subgrade subjected to compressive and tensile loadings. Case Studies in Construction Materials, 15, e00575. doi:10.1016/j.cscm.2021.e00575.

[10] Aneke, F. I., & Onyelowe, K. C. (2022). Applications of preloading pressure on expansive subgrade treated with nano-geopolymer binder for cyclic crack resistance. Nanotechnology for Environmental Engineering, 7(3), 593–607. doi:10.1007/s41204-022-00250-4.

[11] Lu, Z., Fang, R., Yao, H., Hu, Z., & Liu, J. (2018). Evaluation and Analysis of the Traffic Load–Induced Settlement of Roads on Soft Subsoils with Low Embankments. International Journal of Geomechanics, 18(6), 41–56. doi:10.1061/(asce)gm.1943-5622.0001123.

[12] Ikechukwu, A. F., Hassan, M. M., & Moubarak, A. (2021). Swelling stress effects on shear strength resistance of subgrades. International Journal of Geotechnical Engineering, 15(8), 939–949. doi:10.1080/19386362.2019.1656445.

[13] Tang, L. S., Chen, H. K., Sun, Y. L., Zhang, Q. H., & Liao, H. R. (2018). Traffic-load-induced dynamic stress accumulation in subgrade and subsoil using small scale model tests. Geomechanics and Engineering, 16(2), 113–124. doi:10.12989/gae.2018.16.2.113.

[14] Guo, L., Wang, J., Cai, Y., Liu, H., Gao, Y., & Sun, H. (2013). Undrained deformation behavior of saturated soft clay under long-term cyclic loading. Soil Dynamics and Earthquake Engineering, 50(1), 28–37. doi:10.1016/j.soildyn.2013.01.029.

[15] Cai, Y., Sun, Q., Guo, L., Juang, C. H., & Wang, J. (2015). Permanent deformation characteristics of saturated sand under cyclic loading. Canadian Geotechnical Journal, 52(6), 795–807. doi:10.1139/cgj-2014-0341.

[16] Liu, X., Zhang, X., & Wang, X. (2021). Resilient modulus and cumulative plastic strain of frozen silty clay under dynamic aircraft loading. SN Applied Sciences, 3(10), 805. doi:10.1007/s42452-021-04792-1.

[17] Qiu, C., Cao, D., Wang, Z., & Xu, G. (2016). Permanent deformation characteristics of saturated sand reinforced with horizontal-vertical inclusions under cyclic loading. Electronic Journal of Geotechnical Engineering, 21(21), 6545–6554.

[18] Das, N., & Singh, S. K. (2019). Geotechnical behaviour of lateritic soil reinforced with brown waste and synthetic fibre. International Journal of Geotechnical Engineering, 13(3), 287–297. doi:10.1080/19386362.2017.1344002.

[19] Moghal, A. A. B., Basha, B. M., & Ashfaq, M. (2019). Probabilistic Study on the Geotechnical Behavior of Fiber Reinforced Soil. Frontiers in Geotechnical Engineering. Developments in Geotechnical Engineering. Springer, Singapore. doi:10.1007/978-981-13-5871-5_17.

[20] Ibraim, E., Camenen, J. F., Diambra, A., Kairelis, K., Visockaite, L., & Consoli, N. C. (2018). Energy efficiency of fibre reinforced soil formation at small element scale: Laboratory and numerical investigation. Geotextiles and Geomembranes, 46(4), 497–510. doi:10.1016/j.geotexmem.2018.04.008.

[21] Seed, H. B., & Idriss, I. M. (1970). Soil moduli and damping factors for dynamic response analysis. Journal of Terramechanics, 8(3), 109. doi:10.1016/0022-4898(72)90110-3.

[22] AASHTO. (1962). The AASHTO road test, report 5-pavement research. Pavement Research. Accession No. 01417540, Highway Research Board, American Association of State Highway and Transportation Officials (AASHTO), Washington DC, United States.

[23] Brown, S. F., & Hyde, A. F. L. (1975). Significance of cyclic confining stress in repeated-load triaxial testing of granular material. International Journal of Rock Mechanics and Mining Sciences & Geomechanics Abstracts, 13(9), A102. doi:10.1016/0148-9062(76)90013-9.

[24] Ling, J. M., Wang, W., & Wu, H. B. (2002). Residual deformation of saturated clay subgrade under vehicle load. Tongji Daxue Xuebao/Journal of Tongji University, 30(11), 1315–1320. doi:10.3321/j.issn:0253-374X.2002.11.007.

[25] Mazari, M., Navarro, E., Abdallah, I., & Nazarian, S. (2014). Comparison of numerical and experimental responses of pavement systems using various resilient modulus models. Soils and Foundations, 54(1), 36–44. doi:10.1016/j.sandf.2013.12.004.

[26] Yang, M., Men, Y. M., Cao, L., & Yuan, L. Q. (2016). Numerical analysis of stress in soil due to subway moving loads in ground fissure area. Chinese Journal of Underground Space and Engineering, 12 (06), 1545–1552.

[27] Thevakumar, K., Indraratna, B., Ferreira, F. B., Carter, J., & Rujikiatkamjorn, C. (2021). The influence of cyclic loading on the response of soft subgrade soil in relation to heavy haul railways. Transportation Geotechnics, 29, 100571. doi:10.1016/j.trgeo.2021.100571.

[28] ASTM D1140-17. (2017). Standard Test Methods for Determining the Amount of Material Finer than 75-μm (No. 200) Sieve in Soils by Washing. ASTM International, Pennsylvania, United States. doi:10.1520/D1140-17.

[29] ASTM D4318-17e1. (2018). Standard Test Methods for Liquid Limit, Plastic Limit, and Plasticity Index of Soils. ASTM International, Pennsylvania, United States. doi:10.1520/D4318-17E01.

[30] ASTM D3822/D3822M-14. (2020). Standard Test Method for Tensile Properties of Single Textile Fibres. ASTM International, Pennsylvania, United States. doi:10.1520/D3822_D3822M-14R20.

[31] ASTM D698-12. (2007). Standard Test Methods for Laboratory Compaction Characteristics of Soil Using Standard Effort (12400 ft- lbf/ft^3 (600 kN- m/ m^3)). ASTM International, Pennsylvania, United States. doi:10.1520/D0698-12R21.

[32] Bledzki, A. K., Mamun, A. A., Lucka-Gabor, M., & Gutowski, V. S. (2008). The effects of acetylation on properties of flax fibre and its polypropylene composites. Express Polymer Letters, 2(6), 413–422. doi:10.3144/expresspolymlett.2008.50.

[33] AASHTO T307-99. (2003). Standard method of test for determining the resilient modulus of soils and aggregate materials. American Association of State Highway and Transportation Officials (AASHTO), Washington, United States.

[34] Vucetic, M., & Mortezaie, A. (2015). Cyclic secant shear modulus versus pore water pressure in sands at small cyclic strains. Soil Dynamics and Earthquake Engineering, 70, 60–72. doi:10.1016/j.soildyn.2014.12.001.

[35] Salour, F., Erlingsson, S., & Zapata, C. E. (2013). Modelling resilient modulus seasonal variation of Silty sand subgrade soils with matric suction control. Canadian Geotechnical Journal, 51(12), 1413–1422. doi:10.1139/cgj-2013-0484.

[36] Yaghoubi, E., Yaghoubi, M., Guerrieri, M., & Sudarsanan, N. (2021). Improving expansive clay subgrades using recycled glass: Resilient modulus characteristics and pavement performance. Construction and Building Materials, 302, 124384. doi:10.1016/j.conbuildmat.2021.124384.

[37] Gaspard, K., Zhang, Z., Gautreau, G., Hanifa, K., Zapata, C. E., & Abufarsakh, M. (2019). Modeling the Resilient Modulus Variation of in Situ Soils due to Seasonal Moisture Content Variations. Advances in Civil Engineering, 2019. doi:10.1155/2019/1793601.

[38] George, V., & Kumar, A. (2018). Studies on modulus of resilience using cyclic tri-axial test and correlations to PFWD, DCP, and CBR. International Journal of Pavement Engineering, 19(11), 976–985. doi:10.1080/10298436.2016.1230428.

[39] Al Adili, A., Azzam, R., Spagnoli, G., & Schrader, J. (2012). Strength of soil reinforced with fiber materials (Papyrus). Soil Mechanics and Foundation Engineering, 48(6), 241–247. doi:10.1007/s11204-012-9154-z.

[40] Głuchowski, A., & Sas, W. (2020). Long-term cyclic loading impact on the creep deformation mechanism in cohesive materials. Materials, 13(17), 3907. doi:10.3390/ma13173907.

[41] An, R., Kong, L., Shi, W., & Zhang, X. (2022). Stiffness decay characteristics and disturbance effect evaluation of structured clay based on in-situ tests. Soils and Foundations, 62(5), 101184. doi:10.1016/j.sandf.2022.101184.

[42] Kennedy, S., Clarke, S., & Shepley, P. (2022). The Effect of Stress Level on the Resilient Modulus of Non-Engineered Mudrock Backfill Materials. CivilEng, 3(3), 630–642. doi:10.3390/civileng3030037.

[43] Xie, L., Zhao, Z., & Lei, Y. (2019). Accumulated Plastic Strain of Silty Clay under Subway Moving Loads. Journal of Shenyang Jianzhu University (Natural Science), 35(1), 91–100. doi:10.11717/j.issn:2095-1922.2019.01.11.

[44] Sandjak, K., & Tiliouine, B. (2012). Experimental evaluation of non-linear resilient deformations of some algerian aggregates under cyclic loading. Arabian Journal for Science and Engineering, 39(3), 1507–1516. doi:10.1007/s13369-013-0737-4.

[45] Tang, L., Zhao, Z., Chen, H., Wu, Y., & Zeng, Y. (2019). Dynamic stress accumulation model of granite residual soil under cyclic loading based on small-size creep tests. Journal of Central South University, 26(3), 728–742. doi:10.1007/s11771-019-4043-5.

[46] Bian, X., Jiang, J., Jin, W., Sun, D., Li, W., & Li, X. (2016). Cyclic and Postcyclic Triaxial Testing of Ballast and Subballast. Journal of Materials in Civil Engineering, 28(7), 4016032. doi:10.1061/(asce)mt.1943-5533.0001523.

[47] Han, Z., Vanapalli, S. K., Ren, J. ping, & Zou, W. lie. (2018). Characterizing cyclic and static moduli and strength of compacted pavement subgrade soils considering moisture variation. Soils and Foundations, 58(5), 1187–1199. doi:10.1016/j.sandf.2018.06.003.

[48] Estabragh, A. R., Moghadas, M., Moradi, M., & Javadi, A. A. (2017). Consolidation behavior of an unsaturated silty soil during drying and wetting. Soils and Foundations, 57(2), 277–287. doi:10.1016/j.sandf.2017.03.005.

[49] Kumar, S. S., Krishna, A. M., & Dey, A. (2017). Evaluation of dynamic properties of sandy soil at high cyclic strains. Soil Dynamics and Earthquake Engineering, 99, 157–167. doi:10.1016/j.soildyn.2017.05.016.

[50] Soliman, H., & Shalaby, A. (2015). Permanent deformation behavior of unbound granular base materials with varying moisture and fines content. Transportation Geotechnics, 4, 1–12. doi:10.1016/j.trgeo.2015.06.001.

[51] Madhavi Latha., G., & Nandhi Varman., A. M. (2016). Static and cyclic load response of reinforced sand through large triaxial tests. Japanese Geotechnical Society Special Publication, 2(68), 2342–2346. doi:10.3208/jgssp.igs-39.

[52] Ying, M., Liu, F., Wang, J., Wang, C., & Li, M. (2021). Coupling effects of particle shape and cyclic shear history on shear properties of coarse-grained soil–geogrid interface. Transportation Geotechnics, 27, 100504. doi:10.1016/j.trgeo.2020.100504.

[53] Olgun, M. (2013). Effects of polypropylene fiber inclusion on the strength and volume change characteristics of cement-fly ash stabilized clay soil. Geosynthetics International, 20(4), 263–275. doi:10.1680/gein.13.00016.

[54] Gao, L., Zhou, Q., Yu, X., Wu, K., & Mahfouz, A. H. (2017). Experimental study on the unconfined compressive strength of carbon fiber reinforced clay soil. Marine Georesources & Geotechnology, 35(1), 143–148. doi:10.1080/1064119X.2015.1102184.

[55] Tang, C. S., Li, J., Wang, D. Y., & Shi, B. (2016). Investigation on the interfacial mechanical behavior of wave-shaped fiber reinforced soil by pullout test. Geotextiles and Geomembranes, 44(6), 872–883. doi:10.1016/j.geotexmem.2016.05.001.